



**HAL**  
open science

## Reconstruction of uranium and plutonium isotopic signatures in sediment accumulated in the Mano Dam reservoir, Japan, before and after the Fukushima nuclear accident

Hugo Jaegler, Fabien Pointurier, Silvia Diez-Fernández, Alkiviadis Gourgiotis, Hélène Isnard, Seiji Hayashi, Hideki Tsuji, Yuichi Onda, Amelie Hubert, J. Patrick Lacey, et al.

### ► To cite this version:

Hugo Jaegler, Fabien Pointurier, Silvia Diez-Fernández, Alkiviadis Gourgiotis, Hélène Isnard, et al.. Reconstruction of uranium and plutonium isotopic signatures in sediment accumulated in the Mano Dam reservoir, Japan, before and after the Fukushima nuclear accident. *Chemosphere*, 2019, 225, pp.849-858. 10.1016/j.chemosphere.2019.03.064 . hal-02336278

**HAL Id: hal-02336278**

**<https://hal.science/hal-02336278>**

Submitted on 28 Oct 2019

**HAL** is a multi-disciplinary open access archive for the deposit and dissemination of scientific research documents, whether they are published or not. The documents may come from teaching and research institutions in France or abroad, or from public or private research centers.

L'archive ouverte pluridisciplinaire **HAL**, est destinée au dépôt et à la diffusion de documents scientifiques de niveau recherche, publiés ou non, émanant des établissements d'enseignement et de recherche français ou étrangers, des laboratoires publics ou privés.



Distributed under a Creative Commons Attribution 4.0 International License

1 Reconstruction of uranium and plutonium isotopic signatures in  
2 sediment accumulated in the Mano Dam reservoir, Japan, before  
3 and after the Fukushima accident  
4

5 Hugo Jaegler<sup>1</sup>, Fabien Pointurier<sup>2</sup>, Silvia Diez-Fernández<sup>3</sup>, Alkiviadis Gourgiotis<sup>4</sup>, Hélène Isnard<sup>3</sup>, Seiji  
6 Hayashi<sup>5</sup>, Hideki Tsuji<sup>5</sup>, Yuichi Onda<sup>6</sup>, Amélie Hubert<sup>2</sup>, J. Patrick Lacey<sup>1,7</sup> & Olivier Evrard<sup>1\*</sup>

7  
8 **Affiliations:**

9 <sup>1</sup>Laboratoire des Sciences du Climat et de l'Environnement, LSCE/IPSL, UMR 8212 (CEA-CNRS-UVSQ),  
10 Université Paris-Saclay, F-91198 Gif-sur-Yvette Cedex, France

11 <sup>2</sup>CEA, DAM, DIF, F-91297 Arpajon, France

12 <sup>3</sup> Den – Service d'Etudes Analytiques et de Réactivité des Surfaces (SEARS), CEA, Université Paris-  
13 Saclay, F-91191, Gif sur Yvette, France

14 <sup>4</sup>Institut de Radioprotection et de Sûreté Nucléaire - PSE/ENV - SEDRE/LELI BP 17, Fontenay-aux-  
15 Roses, 92262, France

16 <sup>5</sup>National Institute for Environmental Science, Fukushima Branch, 10-2 Fukasaku, Miharu, Tamura,  
17 Fukushima, 963-7700 Japan

18 <sup>6</sup>Center for Research in Isotopes and Environmental Dynamics (CRIED), University of Tsukuba,  
19 Tsukuba, Japan

20 <sup>7</sup>Environmental Monitoring and Science Division, Alberta Environment and Parks, 3115 – 12 Street NE  
21 Calgary, Alberta, Canada

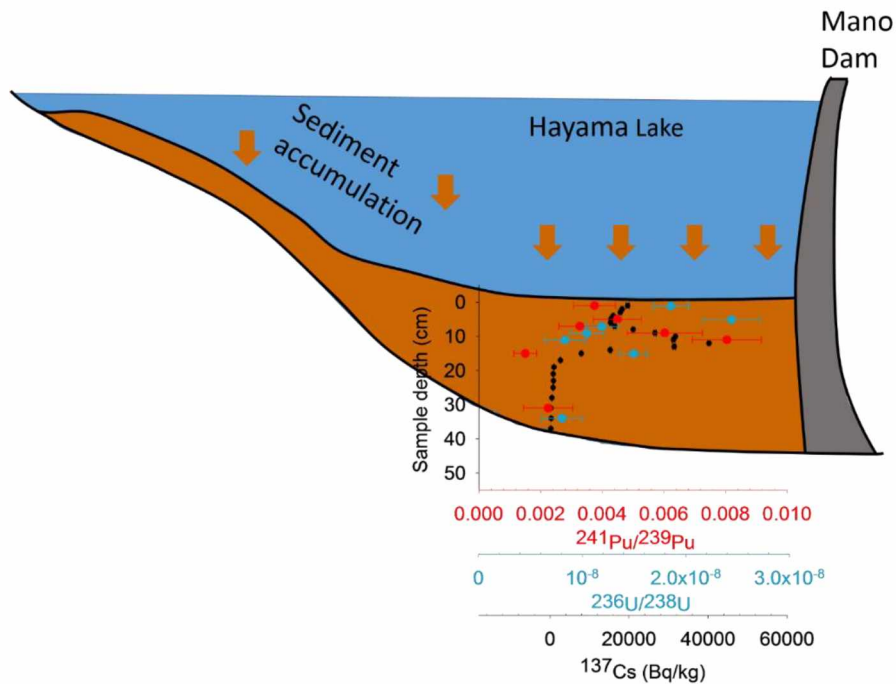
22 (\*) Corresponding author (email address: [olivier.evrard@lsce.ipsl.fr](mailto:olivier.evrard@lsce.ipsl.fr)).

24 **Abstract**

25

26 The Fukushima Dai-ichi Nuclear Power Plant (FDNPP) accident in Japan resulted in a major release of  
27 radionuclides into the environment. Compared to others elements, few studies have investigated the  
28 emission of actinides. Accordingly, this research investigates the Pu composition in soil samples  
29 collected in nearby paddy fields before and after the accident. Furthermore, the vertical distributions  
30 of Pu and U isotopic signatures, along with  $^{137}\text{Cs}$  activities, were measured in a sediment core  
31 collected in 2015 in the Mano Dam reservoir, in the Fukushima Prefecture. These signatures were  
32 used to quantify changes in the relative contributions of the major actinide sources (global fallout or  
33 FDNPP derived fallout) in sediment deposited in the reservoir. The distinct peak observed for all Pu  
34 isotope ratios ( $^{240}\text{Pu}/^{239}\text{Pu}$ ,  $^{241}\text{Pu}/^{239}\text{Pu}$  and  $^{242}\text{Pu}/^{239}\text{Pu}$ ) and for  $^{137}\text{Cs}$  concentrations in the sediment  
35 core was attributed to the Fukushima fallout, and coincided with the maximum atomic contribution  
36 of only  $4.8\pm 1.0\%$  of Pu from the FDNPP. Furthermore,  $^{236}\text{U}/^{238}\text{U}$  ratios measured in the sediment core  
37 remained close to the global fallout signature indicating there was likely no U from the FDNPP  
38 accident in the sediment core. More research is required on the environmental dynamics of trace  
39 actinides in landscapes closer to the FDNPP where greater abundances of FDNPP-derived Pu and U  
40 would be anticipated.

41 **Abstract art**



42

43

44 **Introduction**

45

46 The 2011 Fukushima Dai-ichi Nuclear Power Plant (FDNPP) accident released significant volumes of  
47 radionuclides into the environment. In particular, various venting operations and explosions occurred  
48 at the FDNPP and triggered the release of volatile fission products ( $^{131}\text{I}$ ,  $^{132}\text{Te}$ ,  $^{134}\text{Cs}$  and  
49  $^{137}\text{Cs}$ )(Schneider et al., 2017). Accordingly, numerous studies were conducted to investigate the  
50 distribution and the fate of the gamma-emitting isotopes, including radiocesium, after the  
51 accident(Buesseler et al., 2016; Cao et al., 2016; Tanaka et al., 2015; Yamamoto et al., 2012; Zheng et  
52 al., 2014). Erosion and remobilisation of particle-bound radiocesium contamination was investigated  
53 through field monitoring(Evrard et al., 2016; Yamashiki et al., 2014) and model simulations(Kitamura  
54 et al., 2016; Kitamura et al., 2014). These studies reported a rapid export of the particle-bound  
55 radioactive contamination by the coastal rivers to the Pacific Ocean, with the preferential  
56 remobilisation of fine sediment particles enriched in radiocesium. This process was shown to be

57 exacerbated during heavy typhoons, because of the strong hillslope-to-river sediment connectivity  
58 observed, particularly with paddy fields that were found to be one of the main sources of  
59 radiocesium shortly after the accident(Chartin et al., 2017; Laceby et al., 2016; Lepage et al., 2016).  
60 Importantly, dams and reservoirs were demonstrated to store significant quantities of contaminated  
61 sediment in the region and their management represents a significant challenge for the regional  
62 authorities(Chartin et al., 2013; Yamada et al., 2015).

63 Although radiocesium sources have been extensively researched, less information is available in the  
64 literature regarding the fate of other radionuclides such as U or Pu. Non-volatile Pu isotopes  
65 including  $^{239}\text{Pu}$  ( $T_{1/2}=24,110$  y, alpha-decay),  $^{240}\text{Pu}$  ( $T_{1/2}=6,563$  y, alpha-decay),  $^{241}\text{Pu}$  ( $T_{1/2}=14.35$  y,  
66 beta-decay) and  $^{242}\text{Pu}$  ( $T_{1/2}=376,000$  y, alpha-decay)(Evrard et al., 2014; Xu et al., 2016; Yamamoto et  
67 al., 2014; Zheng et al., 2012b) and U isotopes including  $^{238}\text{U}$  ( $T_{1/2}=4.469\times 10^9$  y, alpha-decay),  $^{235}\text{U}$   
68 ( $T_{1/2}=7.038\times 10^8$  y, alpha-decay),  $^{234}\text{U}$  ( $T_{1/2}=245,500$  y, alpha-decay) and  $^{236}\text{U}$  ( $T_{1/2}=23.42\times 10^6$  y, alpha-  
69 decay)(Sakaguchi et al., 2014; Schneider et al., 2017; Shinonaga et al., 2014; Yang et al., 2016), were  
70 also detected in environmental samples collected in the Fukushima Prefecture. These radionuclides  
71 may originate from two main sources: the global fallout associated with the nuclear atmospheric  
72 weapon tests(Yamamoto et al., 2014) and the FDNPP accident. Additionally,  $^{238}\text{U}$ ,  $^{235}\text{U}$  and  $^{234}\text{U}$   
73 isotopes are naturally present in the environment. As Pu ( $^{240}\text{Pu}/^{239}\text{Pu}$ ,  $^{241}\text{Pu}/^{239}\text{Pu}$  and  $^{242}\text{Pu}/^{239}\text{Pu}$ ) and  
74 U ( $^{236}\text{U}/^{238}\text{U}$ ) isotope ratios may vary significantly depending on their source(Muramatsu et al., 2003;  
75 Schneider et al., 2017), their precise measurement in sediment could provide powerful fingerprints  
76 for source identification. Accordingly, investigating the changes in the Pu and U signatures with  
77 depth in lacustrine sediment cores should provide information for reconstructing the changes in the  
78 respective contributions of these radionuclide sources in lacustrine sediment.

79 To the best of our knowledge, the analysis of Pu isotopes in continental sediment deposited in  
80 reservoirs following the FDNPP accident has been restricted to that of cores collected in the Lake  
81 Inba, located 200 km south of the FDNPP site (i.e. outside of the main radioactive plume)(Cao et al.,  
82 2017). Although the measured  $^{134}\text{Cs}/^{137}\text{Cs}$  ratios indicated there was fallout from the FDNPP accident,

83 the  $^{239+240}\text{Pu}$  activity and the  $^{240}\text{Pu}/^{239}\text{Pu}$  ratio remained similar to the global fallout signature,  
84 suggesting that FDNPP-derived Pu did not reach the Lake Inba basin in significant quantities.

85 In this study, the global fallout signature was first refined for the study region through the analysis of  
86 soil samples collected before the accident. Soils collected after the accident were analysed to  
87 characterise the initial spatial pattern of Pu deposited in this area and to compare it with the well-  
88 documented  $^{137}\text{Cs}$  deposition pattern. Then, the vertical distribution of Pu and U isotope ratios was  
89 characterised in a sediment core. These distributions were compared to that of  $^{137}\text{Cs}$  concentrations  
90 measured in the core, and the contributions of the different sources of Pu in this region (global  
91 fallout vs. FDNPP) were quantified through the analysis of Pu isotope ratios. Implications regarding  
92 the fate and the geochemical behaviour of actinides in the catchments draining the main radioactive  
93 plume in the Fukushima Prefecture are then discussed.

94

## 95 **Materials and methods**

96

### 97 **Soil and sediment sampling**

98

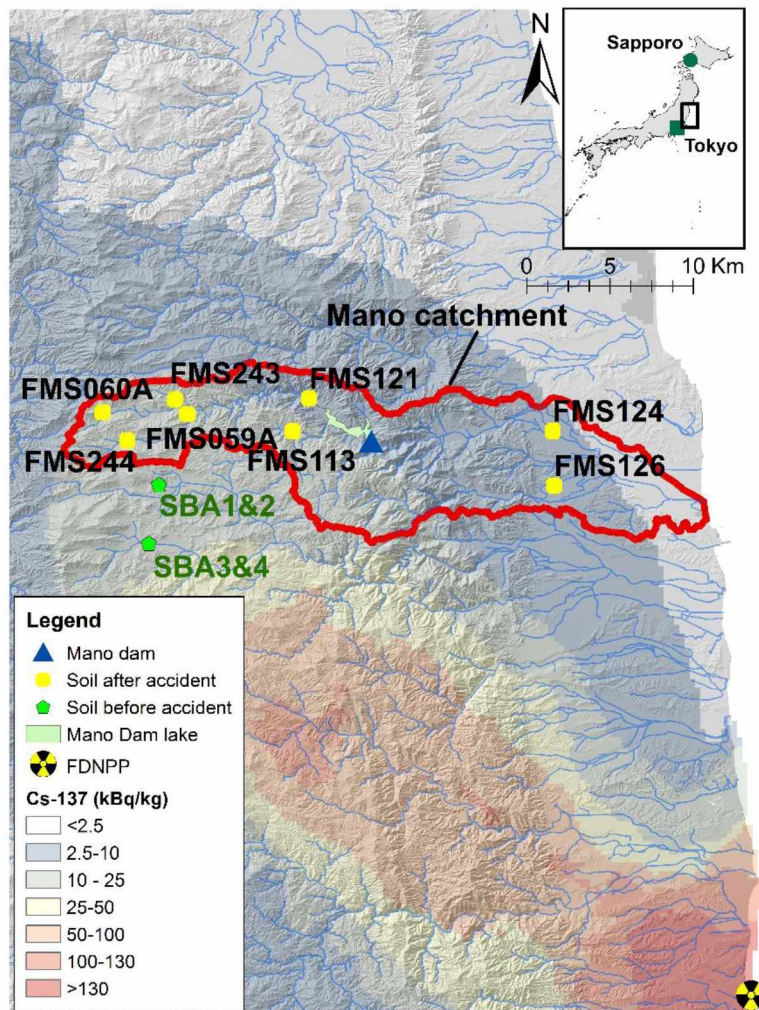
99 In order to provide the local signature of the Pu global fallout in this region, four soil samples  
100 collected before the accident (in 2007 and in 2010, see Table S1) were first analysed. These samples  
101 were taken at two different locations in cultivated paddy fields (12 km to the south-west of the Mano  
102 Dam, see Figure 1) and at two different depths (ploughed and underlying layers). To characterise the  
103 initial deposition of FDNPP-derived Pu, soil samples collected shortly after the accident (in November  
104 2011, November 2012 and April 2012, see Table S2) were also analysed. Soil samples were taken  
105 from a range of  $^{137}\text{Cs}$  fallout levels to be representative of potential FDNPP fallout (see Figure 1).  
106 Sampling methods are described elsewhere (Jaegler et al., 2018). In brief, soil samples are composed

107 of 10 soil scrape subsamples, taken with a plastic trowel, that were thoroughly homogenized prior to  
108 analyses.

109

110 A sediment core collected in Lake Hayama, which is located 39 km to the northwest of the FDNPP in  
111 the Mano River catchment, was analysed. This lake corresponds to the artificial Mano Dam reservoir,  
112 with an area of 1.75 km<sup>2</sup>, a water volume of 36,200 ×10<sup>3</sup> m<sup>3</sup> and a retention time of 0.48  
113 year(Fukushima and Arai, 2014; Matsuda et al., 2015).

114 Researchers have investigated the radioactive contamination of sediment accumulated in this lake,  
115 although they restricted their analysis to radiocesium concentrations. Matsuda *et al.*(2015)  
116 measured the radiocesium concentration in bottom sediment and in lake water samples in 2012 and  
117 2013, and they observed respective concentration decreases of 57% and 43% between the  
118 successive sampling campaigns. Huon *et al.*(2018) measured the vertical distribution of <sup>137</sup>Cs  
119 activities in four sediment cores sampled across the lake. Three of these four cores showed a distinct  
120 peak likely corresponding to the initial radiocesium wash-off and migration phase following the  
121 FDNPP accident. In the current study, one of these sediment cores (referred to as 'DD1') located in  
122 the downstream section of the lake and composed of fine sediment material(Huon et al., 2018) was  
123 selected to characterise variations of Pu and U isotope ratios with depth. More details on the core  
124 sampling and the radiocesium analyses are provided in Huon *et al.*(2018). In brief, the sediment core  
125 was collected on April 24, 2015 (37°43'25.75"N, 140°49'49.84"E) using a gravity core sampler, under  
126 approximately 45 m of water. The sediment core was 37 cm long and was then divided into 1-cm  
127 increments from 0 to 15 cm depth, 2 cm from 15 to 25 cm depth and, finally, 3 cm from 25 to 37 cm  
128 depth. <sup>137</sup>Cs content was measured by gamma spectrometry in each subsample in order to  
129 investigate the distribution of <sup>137</sup>Cs in the core(Huon et al., 2018).



130

131 Figure 1: Location of the soil samples analysed in this current research in the Mano catchment delineated in  
 132 red. The main radiocaesium contamination plume is also located in the background map derived from Chartin  
 133 *et al.*(2013).

134

### 135 Chemical preparation and separation of plutonium and uranium

136

137 Core sections were grouped by pairs to provide sufficient material (~5 g) for the actinide analyses.  
 138 Samples were placed in an electric furnace at 450 °C for ~15 h to decompose the organic matter.  
 139 After cooling to room temperature, they were transferred in Savillex® PFA Teflon® beakers. ~100 fg  
 140 of <sup>244</sup>Pu (diluted solution prepared from the certified isotopic reference material IRMM-042a, Geel,  
 141 Belgium) was added as an isotopic dilution tracer. Chemical blanks were spiked as well. Digestion of



142 the samples was carried out through several acid leaching steps. Only partial dissolution protocol was  
143 performed as it was shown that this partial leaching was sufficient to dissolved actinide contained in  
144 samples(Lee et al., 2005,Liao, 2008 #532,Jaegler, 2018 #970). Moreover, total dissolution required  
145 use of concentrated HF acid, which is known to contain more impurities than concentrated HCl and  
146 HNO<sub>3</sub> acid.

147 50 mL concentrated HNO<sub>3</sub>, 50 mL aqua regia and 50 mL concentrated HCl. Between each leaching  
148 step, the solutions were dried in a closed evaporation system (Evapoclean®, Analab, Hoenheim,  
149 France) at 110 °C until complete dryness. This device allows evaporation in a closed medium to  
150 prevent any lab contamination. Samples were then recovered with 2M HCl and filtrated with a  
151 disposable 0.45 µm Nalgene filtering unit (Thermo Scientific, Rochester, NY, USA). Dissolved fractions  
152 were transferred in clean Savillex® PFA Teflon® beakers and evaporated to dryness in closed media.  
153 Samples were then recovered with 50 mL of concentrated HNO<sub>3</sub> and a few mg of NaNO<sub>2</sub> were added  
154 to stabilize the (+IV) oxidation state of Pu and evaporated to dryness. Samples were finally recovered  
155 with 30 mL of 8M HNO<sub>3</sub> before Pu separation on chromatographic columns. The first column was  
156 composed of a Dowex AG1X8 anion-exchange resin filled with ~10 mL of 50-100 mesh AG1X8 resin  
157 and ~10 mL of 100-200 mesh AG1X8 resin, conditioned with 8 M HNO<sub>3</sub>. After loading the sample  
158 onto the column, U was first eluted with 8M HNO<sub>3</sub>. Then, Th was eliminated with 10 M HCl. Pu was  
159 finally eluted with NH<sub>4</sub>I (1.5%) – 12 M HCl.

160 The same protocol was repeated twice on the Pu fraction with 2 mL Dowex AG1X4 anion-exchange  
161 resin (100-200 mesh) to reduce as much as possible sample matrix elements, which can potentially  
162 generate polyatomic (mainly PbO<sub>2</sub><sup>+</sup>, <sup>238</sup>UH<sup>+</sup>) and isobaric (<sup>241</sup>Am<sup>+</sup>) interferences. After evaporation of  
163 the eluate, samples were recovered and evaporated to dryness several times with concentrated  
164 HNO<sub>3</sub> to eliminate chlorides. Finally, the last recovery was performed with 2% HNO<sub>3</sub> + 0.01M HF for  
165 ICP-MS measurements. The two consecutive purifications of the Pu fraction with Dowex resins  
166 allowed a complete elimination of Am(Trémillon, 1965). However, PbO<sub>2</sub><sup>+</sup> and UH<sup>+</sup> interferences  
167 persisted during ICP-MS measurements and required raw data corrections. The U fraction collected

168 with the first Dowex AG1X8 was further purified with a second column of 2 mL UTEVA extraction  
169 resin (100 – 150 µm), conditioned with 4M HNO<sub>3</sub>. U was directly eluted with 0.01M HNO<sub>3</sub>. After  
170 evaporation to dryness of this eluted solution, the U fraction of samples was finally recovered with  
171 2% HNO<sub>3</sub> for ICP-MS measurements. At least two chemical blanks were systematically prepared with  
172 sample treatments. **The sample preparation and Pu and U separation protocol efficiency was confirm**  
173 **by analysing certified reference materials in a previous study (Jaegler et al., 2018).**

#### 174 **Plutonium measurements by mass-spectrometry**

175  
176 Pu isotopic composition in the samples were measured with a Multi-Collector Inductively Coupled  
177 Plasma Mass Spectrometer (MC-ICP-MS) (Neptune Plus, Thermo Fisher Scientific Inc., Bremen,  
178 Germany) equipped with eight Faraday cups and five ion counters for the simultaneous detection of  
179 ion beams. All measurements were performed using Aridus II (Cetac) as introduction system, high-  
180 efficiency sampler and skimmer cones, reinforced pumping in the interface to enhance the sensitivity  
181 by a factor of ~10 (approximately 10<sup>8</sup> counts/s per µg/L of <sup>238</sup>U), compared to the standard  
182 configuration.

183 Two certified reference materials, IRMM 186 and IRMM 057 (both reference materials were  
184 provided by the Institute for Reference Materials and Measurements, Geel, Belgium), were  
185 measured on a regular basis throughout each analysis sequence and used to correct interferences  
186 and biases: instrumental mass fractionation, peak tailing at M+1 and M+2, and hydride formation  
187 (mainly <sup>238</sup>UH<sup>+</sup>) were determined. **Lead polyatomic interferences (PbO<sub>2</sub><sup>+</sup>) were corrected by**  
188 **measuring three pure mono-elemental solutions of Pb at the end of the procedure. Measurement of**  
189 **these standards in the chemical blanks shows that main lead interferences are instrumental induced**  
190 **(PbAr) rather than induced by the chemical protocol (PbCl). Moreover, as levels of interferences as**  
191 **similar in the blanks and in the sample, it shows that Pb is originating from the reagents added during**  
192 **radiochemical protocol and not contained in the sample.** All these corrections were applied to a

193 solution of the Pu isotopic certified material CRM128 (NBL, US DOE) for verification. Finally, all Pu  
194 compositions were corrected for tracer impurities according to the certificate of the isotopic  
195 reference material IRMM-042a, decay-corrected to March 15, 2011 and for blank levels (average of  
196 total Pu in the blanks:  $3.4 \pm 1.2$  fg).

197

## 198 **Uranium measurements by mass spectrometry**

199

200 Precise  $^{236}\text{U}$  measurements were performed twice in two different laboratories: at CEA/LANIE  
201 (“Commissariat à l’Energie Atomique et aux Energies Alternatives/ Laboratoire de développement  
202 Analytique Nucléaire, Isotopique, Élémentaire”) and at IRSN/LELI (“Institut de Radioprotection et de  
203 Sûreté du Nucléaire / Laboratoire sur le devenir des pollutions des sites radioactifs”) using two ICP-  
204 MS/MS (Agilent 8800, Agilent Technologies, Tokyo, Japan) instruments well-suited for the  
205 measurement of extremely low  $^{236}\text{U}/^{238}\text{U}$  isotope ratios (Tanimizu et al., 2013; Yang et al., 2016). Two  
206 analyses on each sample were conducted to provide more confidence in the results. The strategy  
207 followed in both laboratories was based on the mass shift mode (through the detection of the oxide  
208 form,  $\text{U}^{16}\text{O}^+$ ) as described by Tanimizu *et al.* and Yang *et al.* (2013; 2016). This strategy allowed for  
209 reducing  $^{238}\text{U}$  and  $^{235}\text{U}$  peak tailing and hydride formation from  $^{235}\text{U}$  at  $m/z=236$  opening up the  
210 possibility to measure very low  $^{236}\text{U}/^{238}\text{U}$  isotope ratios. Owing to these strong interferences, the  
211 measurement of very low  $^{236}\text{U}/^{238}\text{U}$  ratios by MC-ICP-MS is limited.

212 Both laboratories are equipped with the same ICP-MS/MS instrument and used desolvating  
213 introduction systems in order to increase sensitivity and to reduce the formation of hydrides.  
214 However, desolvating devices and measurement procedures showed significant differences.

215 The LANIE laboratory used the Aridus (Cetac Technologies, Omaha, NE, USA) introduction system.  
216 The  $^{236}\text{U}/^{238}\text{U}$  in the samples was deduced through the measurement of  $^{236}\text{UO}^+ / ^{235}\text{UO}^+$  using the  
217 natural  $^{238}\text{U}/^{235}\text{U}$  (137.88) ratio (as  $^{238}\text{U}$  and  $^{235}\text{U}$  are mostly originating from natural uranium).

218  $^{236}\text{UO}^+ / ^{235}\text{UO}^+$  ratio was corrected for hydride formation ( $^{235}\text{UOH}^+ / ^{235}\text{UO}^+$ ) and for the chemical  
219 blanks. The instrumental mass fractionation was internally corrected using the  $^{234}\text{UO}^+ / ^{235}\text{UO}^+$  ratios of  
220 the samples, compared with the  $^{234}\text{U} / ^{235}\text{U}$  isotope ratio also determined with another ICP-MS  
221 instrument.

222 The LELI laboratory used the Apex-HF (Elemental Scientific, Omaha, NE, USA) introduction system. In  
223 order to acquire signals only with the pulse counting mode during the analysis, the  $^{236}\text{UO}^+ / ^{235}\text{UO}^+$   
224 ratio was measured and the  $^{236}\text{U} / ^{238}\text{U}$  was deduced using the natural  $^{238}\text{U} / ^{235}\text{U}$  (137.88) ratio.  
225 Instrumental mass fractionation was corrected by a standard bracketing method using the measured  
226  $^{234}\text{U} / ^{235}\text{U}$  ratio of an IRMM186 certified solution. A hydride correction factor was calculated using the  
227  $^{238}\text{UOH}^+ / (^{235}\text{UO}^+ \times 137.88)$  ratio and applied to the  $^{236}\text{U}$  measurements to correct for the  $^{235}\text{UO}^+$   
228 hydride formation.

#### 229 **Pu and U source term signatures**

230

231 Pu deposition on soils of this region may originate from two main sources: the global fallout and the  
232 FDNPP accident. Pu fuel isotopic compositions at the moment of the accident were estimated to be  
233  $0.373 \pm 0.044$  ( $2\sigma$ ) for  $^{240}\text{Pu} / ^{239}\text{Pu}$ ,  $0.1874 \pm 0.0081$  ( $2\sigma$ ) for  $^{241}\text{Pu} / ^{239}\text{Pu}$ , and  $0.0637 \pm 0.0026$  ( $2\sigma$ ) for  
234  $^{242}\text{Pu} / ^{239}\text{Pu}$  (Kirchner et al., 2012; Nishihara et al., 2012; Schwantes et al., 2012).

235 The global fallout signatures provided in the literature were measured worldwide (Kelley et al., 1999)  
236 including various locations across Japan (Momoshima et al., 1997; Muramatsu et al., 2003; Ohtsuka et  
237 al., 2004; Zhang et al., 2010). As the range of these Pu signatures is relatively wide (Table S3), there is  
238 a need to refine the global fallout signatures for this specific sampling location in the Fukushima  
239 Prefecture. In this study, the measurements conducted on the bottom sediment sample layer in the  
240 core and on the soil samples collected before the accident were used to provide the local signatures  
241 of the global fallout.

242 Unlike Pu, U is also naturally present in the environment with two primordial isotopes ( $^{238}\text{U}$  and  $^{235}\text{U}$ )  
243 and one radiogenic isotope ( $^{234}\text{U}$ ) originating from the  $^{238}\text{U}$ -decay. Moreover, these isotopes are  
244 relatively abundant in soils and sediment, with the U concentration being 6 to 9 orders of magnitude  
245 higher than that of Pu(Bu et al., 2017). On the contrary, the  $^{236}\text{U}$  isotope has an extremely low  
246 abundance in natural-occurring U present in environmental samples ( $<10^{-13}$ ). However,  $^{236}\text{U}$  is also  
247 produced in significant quantities in nuclear reactors (by the capture of a neutron by the fissile  
248 nuclide  $^{235}\text{U}$ ), which may result in  $^{236}\text{U}/^{238}\text{U}$  ratios locally higher in those samples collected in the  
249 close vicinity of some nuclear installations. For the U ratio representative of the FDNPP signature,  
250 only Nishihara et al.(2012) estimated the  $^{236}\text{U}/^{238}\text{U}$  in the nuclear fuel ratio at the time of the  
251 accident, being  $(3.20 - 3.71) \times 10^{-3}$  (mean  $(3.42 \pm 0.52) \times 10^{-3}$ ,  $2\sigma$ ). Nevertheless, the main  
252 contribution of  $^{236}\text{U}$  in soils is, as for Pu isotopes, the global fallout associated with the nuclear  
253 weapon atmospheric tests.

254 The representative  $^{236}\text{U}/^{238}\text{U}$  ratios for the global fallout signature in Japan were previously measured  
255 in a soil core (n=3) sampled in the Ishikawa Prefecture(Sakaguchi et al., 2009) ( $1.85 \times 10^{-8} - 1.09 \times 10^{-7}$ ,  
256 mean  $(5.31 \pm 0.12) \times 10^{-8}$ ,  $2\sigma$ ). However, Schneider et al.(2017) recently determined even lower  
257  $^{236}\text{U}/^{238}\text{U}$  ratios in the range of  $10^{-9}$  in soil samples collected at various locations within the exclusion  
258 zone nearby the FDNPP, and reported this signature as that of 'undisturbed uranium'. Currently, this  
259 ratio remains poorly constrained with values varying between  $10^{-10}$  and  $10^{-7}$ .

260 The potential occurrence of U contamination following the FDNPP accident in the environment has  
261 been examined in very few studies(Sakaguchi et al., 2014; Schneider et al., 2017; Shinonaga et al.,  
262 2014; Yang et al., 2016) (See Table S4). Most of these samples reported  $^{236}\text{U}/^{238}\text{U}$  ratios between  $10^{-8}$   
263 and  $10^{-7}$ , which suggests a global fallout origin(Sakaguchi et al., 2010). Shinonaga et al.(2014)  
264 measured ratios of  $10^{-6}$  in aerosol filter samples collected at 120 km from the FDNPP shortly after the  
265 accident. However, as early as in April 2011 U ratios measured in aerosols collected at the same  
266 location returned to the global fallout level. These results suggested that U was only released in trace  
267 amounts during the FDNPP accident.

268

269 Accordingly, in the current research, the U isotope compositions were only analysed in the sediment  
270 core, as the soil erosion and sediment transport processes are known to be selective and to mobilize  
271 preferentially the finest and most contaminated particles(Evrard et al., 2015; Laceby et al., 2017).  
272 Furthermore, <sup>236</sup>U concentrations in the soil samples collected before and after the accident would  
273 likely be too low to be detectable by ICP-MS with the chemical processes followed in this study.

274

### 275 **Quantifying source contributions**

276

277 The proportions of each source of Pu were determined using a binary mixing model(Kelley et al.,  
278 1999). To this end, the isotopic abundance of <sup>241</sup>Pu in each source term and in each sediment sample  
279 and each soil sample collected after the accident was calculated. <sup>241</sup>Pu abundance was used owing to  
280 its relatively short half-life resulting in this isotope providing the best discrimination between  
281 emissions from the global fallout or the FDNPP accident. Atomic abundance of each term  
282  $Ab(^{241}\text{Pu})_{\text{sample}}$ ,  $Ab(^{241}\text{Pu})_{\text{GF}}$  or  $Ab(^{241}\text{Pu})_{\text{FDNPP}}$  is given in Equation 1:

$$Ab(^{241}\text{Pu})_i = \frac{(^{241}\text{Pu}/^{239}\text{Pu})_i}{1 + (^{240}\text{Pu}/^{239}\text{Pu})_i + (^{241}\text{Pu}/^{239}\text{Pu})_i + (^{242}\text{Pu}/^{239}\text{Pu})_i} \quad (1)$$

283 where  $i$  stands for “sample” or “GF” or “FDNPP”.

284 Abundance for FDNPP source  $Ab(^{241}\text{Pu})_{\text{FDNPP}}$  as estimated at  $(1.15 \pm 0.12) \times 10^{-2}$  based on results  
285 published by Nishihara et al.(2012), Kirchner et al.(2012) and Schwantes et al.(2012). Other end-  
286 member abundances were derived from our measurements. Then, the proportions of each source  
287 term were deduced using a mixing equation with two sources (Equation 2):

$$Ab(^{241}\text{Pu})_{\text{FDNPP}} \times X_{\text{FDNPP}} + Ab(^{241}\text{Pu})_{\text{GF}} \times (1 - X_{\text{FDNPP}}) = Ab(^{241}\text{Pu})_{\text{sample}} \quad (2)$$

288 It is important to note that  $X_{\text{FDNPP}}$  is defined based on the total plutonium counting rates (equation  
289 3):

$$X_{\text{FDNPP}} = \frac{({}^{239}\text{Pu} + {}^{240}\text{Pu} + {}^{241}\text{Pu} + {}^{242}\text{Pu})_{\text{FDNPP}}}{({}^{239}\text{Pu} + {}^{240}\text{Pu} + {}^{241}\text{Pu} + {}^{242}\text{Pu})_{\text{sample}}} \quad (3)$$

290

291 These proportions, based on the atomic ratio, were converted into mass proportions to determine  
292 the Pu concentrations originating from the FDNPP relative to those derived from the global fallout.

293 Although no source contribution could be modelled for U, theoretical  ${}^{236}\text{U}$  concentrations released  
294 from the FDNPP were estimated based on the results of plutonium concentrations found in the  
295 samples analysed in the current research. First, the corresponding theoretical  
296  ${}^{236}\text{U}/({}^{239}\text{Pu} + {}^{240}\text{Pu} + {}^{241}\text{Pu} + {}^{242}\text{Pu})$  isotope ratios were estimated to be  $0.46 \pm 0.12$  ( $2\sigma$ ) (Nishihara et al.,  
297 2012), based on literature data. Then, the concentration of FDNPP-derived  ${}^{236}\text{U}$  ( ${}^{236}\text{U}_{\text{FDNPP}}$ ) was  
298 estimated based on the estimations of the FDNPP-derived Pu concentrations found in the soil  
299 samples, and compared with the global fallout derived  ${}^{236}\text{U}$  concentration.

## 300 Results and discussion

301

### 302 Refining the Pu global fallout signature in soils and sediment of the Fukushima Prefecture

303

304 In the sediment core collected in the Hayama Lake, the  ${}^{240}\text{Pu}/{}^{239}\text{Pu}$ ,  ${}^{241}\text{Pu}/{}^{239}\text{Pu}$  and the  ${}^{242}\text{Pu}/{}^{239}\text{Pu}$   
305 isotope ratios measured in the bottom layer (31 cm, MD7) were within the range of values for the  
306 global fallout reported in the literature. Accordingly, it is assumed that these actinides in the bottom  
307 layer of the core were likely supplied by the global fallout.

308 In the soil samples collected before the accident, no Pu was detected in the SBA4 sample (Table 1).

309 Pu isotope ratios found in other samples are surprisingly higher and more heterogeneous than the

310 values previously published in the literature, particularly for the  $^{241}\text{Pu}/^{239}\text{Pu}$  ratio, which ranged from  
 311 0.0023 to 0.0117 (mean  $0.0061 \pm 0.0010$ ,  $2 \sigma$ ). The relative proximity of the sites where Chinese  
 312 nuclear weapons were tested between 1964 and 1980 may have resulted in these high values.  
 313 However, the maximum  $^{241}\text{Pu}/^{239+240}\text{Pu}$  activity ratio measured in the current study is  $61 \pm 12$  (SBA2,  
 314 decay-corrected to the date of the main test on November 17, 1976), which is higher than that  
 315 measured in the Chinese test debris (11 according to Zhang *et al.*, (2010) and Hirose *et al.* (2001)).  
 316 More research is required to investigate these high pre-FDNPP accident plutonium isotope ratio  
 317 values and their heterogeneity.

318

319 Table 1:  $^{137}\text{Cs}$  activities and Pu isotope ratios measured in the soil samples collected before the accident.

320  $^{241}\text{Pu}/^{239}\text{Pu}$  is decay-corrected to March 15, 2011. Uncertainties are extended with a coverage factor of 2.

| Sample label | $^{137}\text{Cs}$ (Bq/kg) | $^{240}\text{Pu}/^{239}\text{Pu}$ | $^{241}\text{Pu}/^{239}\text{Pu}$ | $^{242}\text{Pu}/^{239}\text{Pu}$ | Pu concentration (fg/g) |
|--------------|---------------------------|-----------------------------------|-----------------------------------|-----------------------------------|-------------------------|
| SBA1         | 5.0 ± 1.4                 | 0.182 ± 0.012                     | 0.0044 ± 0.0017                   | 0.0056 ± 0.0010                   | 48.1 ± 5.9              |
| SBA2         | 3.7 ± 0.8                 | 0.179 ± 0.007                     | 0.0117 ± 0.0023                   | 0.0071 ± 0.0006                   | 29.5 ± 1.1              |
| SBA3         | 3.1 ± 1.2                 | 0.179 ± 0.013                     | 0.0023 ± 0.0005                   | 0.0052 ± 0.0013                   | 22.4 ± 1.8              |
| SBA4         | < 2.8                     | -                                 | -                                 | -                                 | < 0.5                   |

321

322 To model the source contributions of Pu in the samples, the Pu isotope ratios characterising the local  
 323 signature of the global fallout in the Mano River catchment was calculated based on those results  
 324 obtained for samples exposed only to the global fallout: the pre-accident soil samples (SBA1, SBA2  
 325 and SBA3) and the bottom layer of the sediment core (MD7). Accordingly, the mean plutonium  
 326 isotope ratios characterising the global fallout signature in the study area are:  $^{240}\text{Pu}/^{239}\text{Pu} = 0.180 \pm$   
 327  $0.010$ ;  $^{241}\text{Pu}/^{239}\text{Pu} = 0.0052 \pm 0.0017$  and  $^{242}\text{Pu}/^{239}\text{Pu} = 0.0054 \pm 0.0022$  (uncertainties are extended  
 328 with a coverage factor of 2.)

329



330 **Initial surface deposition of plutonium in the Mano catchment**

331

332 Pu isotope ratios were measured in eight soil samples collected in the catchment after the accident  
333 (Table 2). Results showed that Pu isotope ratios remained generally close to the global fallout  
334 signature: the atomic proportions of Pu from the FDNPP in these soils were estimated to be lower  
335 than 7 % (see Table 2, Table S5). Sample FMS243 provides an exception to this rule, as it contained  
336 more than 40 % of Pu from the power plant. On the contrary, low isotope ratios were measured in  
337 sample FMS113, in particular the  $^{240}\text{Pu}/^{239}\text{Pu}$  isotope ratio ( $0.160 \pm 0.011$ ). The relevance of this value  
338 is confirmed by the measurement of similar ratios in Japanese soils: Muramatsu *et al.*(2003)  
339 observed a ratio of  $0.155 \pm 0.003$  in a forest soil sample collected before 2002, and Zheng *et*  
340 *al.*(2012b) found a ratio of  $0.144 \pm 0.006$  in a soil sample collected in 2011 at 32 km from the FDNPP.  
341 Moreover, no correlation ( $p < 0.001$ ) could be observed between  $^{137}\text{Cs}$  activities and Pu isotope ratios  
342 in these samples. This confirms that Pu deposition on soils was locally heterogeneous (Salbu, 2011 ;  
343 Schneider *et al.*, 2013). It may also reflect the occurrence of different processes of aerial transport of  
344 radiocesium and Pu from the FDNPP to the study area.

345 Table 2: <sup>137</sup>Cs activities and Pu isotope ratios measured in the soil samples collected after the FDNPP accident across the Mano River catchment. Uncertainties are extended  
 346 with a coverage factor of 2.

| Sample label | <sup>137</sup> Cs (kBq/kg) | <sup>240</sup> Pu/ <sup>239</sup> Pu | <sup>241</sup> Pu/ <sup>239</sup> Pu | <sup>242</sup> Pu/ <sup>239</sup> Pu | Pu concentration (fg/g) | Fraction of Pu from FDNPP (%) |
|--------------|----------------------------|--------------------------------------|--------------------------------------|--------------------------------------|-------------------------|-------------------------------|
| FMS059A      | 18.70 ± 0.94               | 0.177 ± 0.014                        | 0.0033 ± 0.0017                      | 0.0048 ± 0.0019                      | 112.1 ± 6.1             | 1.4 ± 1.2                     |
| FMS060A      | 30.59 ± 1.50               | 0.184 ± 0.017                        | 0.0075 ± 0.0045                      | 0.0059 ± 0.0016                      | 45.8 ± 3.9              | 4.4 ± 3.3                     |
| FMS243       | 19.40 ± 0.97               | 0.285 ± 0.049                        | 0.0666 ± 0.0178                      | 0.0488 ± 0.0029                      | 75.6 ± 9.6              | 40.6 ± 11.4                   |
| FMS244       | 65.72 ± 3.30               | 0.188 ± 0.019                        | 0.0069 ± 0.0009                      | 0.0057 ± 0.0010                      | 78.4 ± 6.0              | 3.9 ± 0.8                     |
| FMS113       | 13.37 ± 0.67               | 0.160 ± 0.011                        | 0.0058 ± 0.0018                      | 0.0075 ± 0.0029                      | 61.0 ± 6.2              | 3.2 ± 1.4                     |
| FMS121       | 0.19 ± 0.01                | 0.184 ± 0.011                        | 0.0027 ± 0.0017                      | 0.0057 ± 0.0007                      | 48.0 ± 3.5              | 0.9 ± 1.3                     |
| FMS124       | 3.28 ± 0.16                | 0.197 ± 0.013                        | 0.0113 ± 0.0062                      | 0.0116 ± 0.0008                      | 67.4 ± 5.4              | 7.0 ± 4.5                     |
| FMS126       | 0.84 ± 0.04                | 0.187 ± 0.016                        | 0.0094 ± 0.0010                      | 0.0124 ± 0.0022                      | 26.1 ± 2.0              | 5.7 ± 1.0                     |

347

348

349 **Temporal variations of radiocesium in the sediment core**

350

351 The  $^{137}\text{Cs}$  activities in the sediment core demonstrated that the lowest activity (mean =  $0.58 \pm 0.03$  Bq/g)  
352 was found in the bottom of the core (at 31 – 37 cm depth). The maximum activity was observed at 11 –  
353 12 cm ( $40.24 \pm 2.01$  Bq/g) before decreasing in the upper part of the core (at 0-7 cm depth) to a mean of  
354  $16.96 \pm 0.85$  Bq/g (Table 3). The maximum of activity corresponds to the deposition of strongly  
355 contaminated sediment in the reservoir shortly after the FDNPP accident. This increase of the activity  
356 likely reflects the radiocesium wash-off and migration phase during the six first months that followed the  
357 FDNPP accident([Huon et al., 2018](#)).

358

359 Table 3:  $^{137}\text{Cs}$  activities and Pu isotope ratios and Pu concentrations measured in the Mano Dam sediment core.

360 Uncertainties are extended with a coverage factor of 2.

| Sample depth (cm) | Sample ID | $^{137}\text{Cs}$ (kBq/kg) | $^{240}\text{Pu}/^{239}\text{Pu}$ | $^{241}\text{Pu}/^{239}\text{Pu}$ | $^{242}\text{Pu}/^{239}\text{Pu}$ | Pu concentration (fg/g) |
|-------------------|-----------|----------------------------|-----------------------------------|-----------------------------------|-----------------------------------|-------------------------|
| 0-1               | MD1       | 19.67 ± 0.98               | 0.180 ± 0.002                     | 0.0038 ± 0.0007                   | 0.0043 ± 0.0003                   | 155.5 ± 11.3            |
| 1-2               |           | 18.27 ± 0.91               |                                   |                                   |                                   |                         |
| 2-3               | -         | 17.77 ± 0.89               | -                                 | -                                 | -                                 | -                       |
| 3-4               | -         | 15.99 ± 0.80               | -                                 | -                                 | -                                 | -                       |
| 4-5               | -         | 15.39 ± 0.77               | -                                 | -                                 | -                                 | -                       |
| 5-6               | MD2       | 15.31 ± 0.77               | 0.172 ± 0.002                     | 0.0045 ± 0.0008                   | 0.0060 ± 0.0004                   | 233.8 ± 21.0            |
| 6-7               |           | 16.35 ± 0.82               |                                   |                                   |                                   |                         |
| 7-8               | MD3       | 21.06 ± 1.05               | 0.174 ± 0.002                     | 0.0033 ± 0.0007                   | 0.0042 ± 0.0003                   | 170.3 ± 25.3            |
| 8-9               |           | 26.55 ± 1.33               |                                   |                                   |                                   |                         |
| 9-10              | MD4       | 31.76 ± 1.59               | 0.184 ± 0.002                     | 0.0060 ± 0.0012                   | 0.0054 ± 0.0005                   | 123.0 ± 12.6            |
| 10-11             |           | 31.23 ± 1.56               |                                   |                                   |                                   |                         |
| 11-12             | MD5       | 40.24 ± 2.01               | 0.182 ± 0.002                     | 0.0080 ± 0.0011                   | 0.0062 ± 0.0003                   | 77.5 ± 12.1             |
| 12-13             |           | 31.43 ± 1.57               |                                   |                                   |                                   |                         |
| 13-14             | -         | 15.22 ± 0.76               | -                                 | -                                 | -                                 | -                       |
| 14-15             | -         | 7.91 ± 0.40                | -                                 | -                                 | -                                 | -                       |
| 15-17             | MD6       | 2.64 ± 0.13                | 0.159 ± 0.001                     | 0.0015 ± 0.0004                   | 0.0034 ± 0.0005                   | 209.1 ± 32.5            |
| 17-19             |           | 0.99 ± 0.05                |                                   |                                   |                                   |                         |
| 19-21             | -         | 0.81 ± 0.04                | -                                 | -                                 | -                                 | -                       |
| 21-23             | -         | 0.88 ± 0.04                | -                                 | -                                 | -                                 | -                       |
| 23-25             | -         | 0.77 ± 0.04                | -                                 | -                                 | -                                 | -                       |
| 25-28             | -         | 0.48 ± 0.02                | -                                 | -                                 | -                                 | -                       |
| 28-31             | -         | 0.24 ± 0.01                | -                                 | -                                 | -                                 | -                       |
| 31-34             | MD7       | 0.29 ± 0.01                | 0.175 ± 0.002                     | 0.0022 ± 0.0008                   | 0.0037 ± 0.0003                   | 84.1 ± 11.4             |
| 34-37             |           | 0.21 ± 0.01                |                                   |                                   |                                   |                         |

361

### 362 Change of plutonium isotopic composition with depth

363

364 The evolution of the Pu isotopic composition with depth showed a similar pattern as  $^{137}\text{Cs}$  activity (see

365 Table 3 and Figure 2). All isotope ratios ( $^{240}\text{Pu}/^{239}\text{Pu}$ ,  $^{241}\text{Pu}/^{239}\text{Pu}$  and  $^{242}\text{Pu}/^{239}\text{Pu}$ ) had a low value at the

366 bottom of the core. Then, all ratios increased up to maximum values found at 11-12 cm depth, which

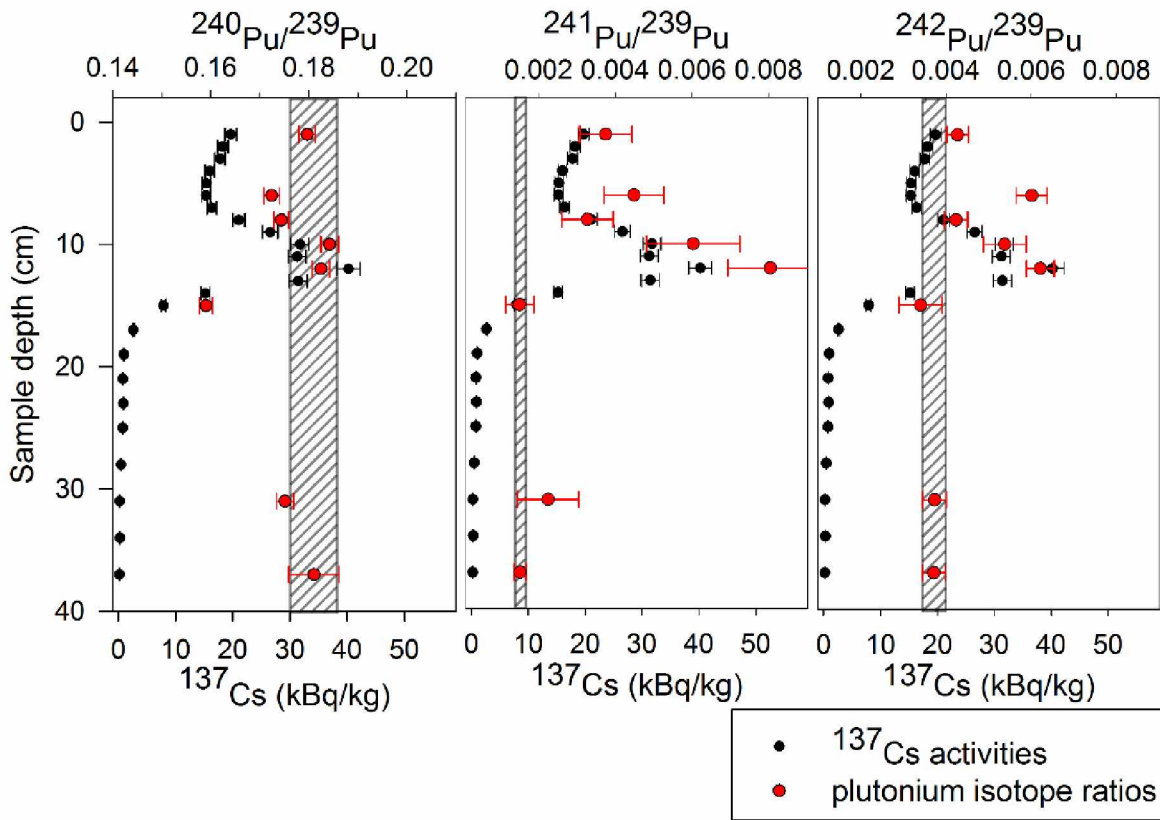
367 corresponds to the peak in the  $^{137}\text{Cs}$  activity. The variations on the sediment core with depth clearly

368 reflect changes in the origin of Pu(Evrard et al., 2014; Jaegler et al., 2018), ranging between the global  
369 fallout signature and the FDNPP signature (see Figure S1), with the exception of the  $^{240}\text{Pu}/^{239}\text{Pu}$  isotope  
370 ratio measured in one sample (see below).

371

372 For  $^{240}\text{Pu}/^{239}\text{Pu}$  ratios, all values remained in the range of the global fallout (Figure 2) although the  
373 highest ratios corresponded to the maximum  $^{137}\text{Cs}$  activity observed in the 11-12 cm depth layer. A  
374 surprisingly low ratio value of  $0.159 \pm 0.001$  was found in the layer MD6 (15 – 19cm depth). Similar ratios  
375 lower than or equal to 0.16 were previously reported in Japan: Muramatsu *et al.*([2003](#)) and Zheng *et*  
376 *al.*([2012b](#)), and Evrard *et al.*([2014](#)), who measured a ratio of  $0.150 \pm 0.005$  in a sediment sample  
377 collected in 2012. For those  $^{241}\text{Pu}/^{239}\text{Pu}$  atom ratios, all isotope ratios measured in sediment samples  
378 collected between 0 and 10 cm depth in the core were significantly higher than the upper limit of the  
379 global fallout signature updated in the current study, showing a clear influence of the FDNPP inputs. A  
380 good correlation was observed between this ratio in particular and the  $^{137}\text{Cs}$  activities (correlation  
381 coefficient of 0.90,  $p$ -value < 0.001). Finally, when examining  $^{242}\text{Pu}/^{239}\text{Pu}$  values, they were slightly higher  
382 than the upper limit of the global fallout, demonstrating a very low, although clear, impact of the FDNPP  
383 fallout.

384



385  
 386 Figure 2: Evolution of  $^{137}\text{Cs}$  activities (black dots),  $^{240}\text{Pu}/^{239}\text{Pu}$ ,  $^{241}\text{Pu}/^{239}\text{Pu}$  and  $^{242}\text{Pu}/^{239}\text{Pu}$  atom ratios (red dots) with  
 387 depth in the Mano Dam sediment core. The dashed zones provide the corresponding range of values reported for  
 388 the global fallout, according to the literature (Kelley et al., 1999; Momoshima et al., 1997; Muramatsu et al., 2003;  
 389 Ohtsuka et al., 2004; Zhang et al., 2010). Uncertainties are extended with a coverage factor of 2.

390  
 391 **Sources of plutonium in the sediment core**  
 392  
 393 The maximum isotope ratio (MD5) corresponded to a maximum FDNPP atomic contribution estimated to  
 394 be  $4.3 \pm 1.0$  %. The measurement conducted on the deeper MD6 sediment layer showed the absence of  
 395 contribution from FDNPP ( $0.0 \pm 0.7$  %). This result suggested that the migration of Pu with depth in the  
 396 sediment profile was negligible.

397 Although detectable, the release of Pu from the FDNPP remained low in the sediment accumulated in  
398 the Mano Dam (Table S6). Accordingly, the Pu detected in the sediment samples was mainly supplied by  
399 the global fallout.

400 The shape of the three Pu isotopes profiles shows the occurrence of large variations, which were not  
401 observed for the  $^{137}\text{Cs}$  activity profile. No correlation ( $p=0.015$ ) was found between  $^{137}\text{Cs}$  and Pu  
402 concentrations, as the main source that supplied these two radionuclides strongly differed:  $^{137}\text{Cs}$  was  
403 mainly supplied by the FDNPP releases, whereas Pu mainly originated from the global fallout. The  
404 variations of Pu in the core likely reflect the heterogeneity of the Pu isotope ratios derived from the  
405 global fallout as the global fallout Pu concentration was shown to be strongly heterogeneous(Kelley et  
406 al., 1999) due to the particulate form of deposition(Salbu, 2011).

407

#### 408 **Evolution of the $^{236}\text{U}$ isotopic signature in the sediment core**

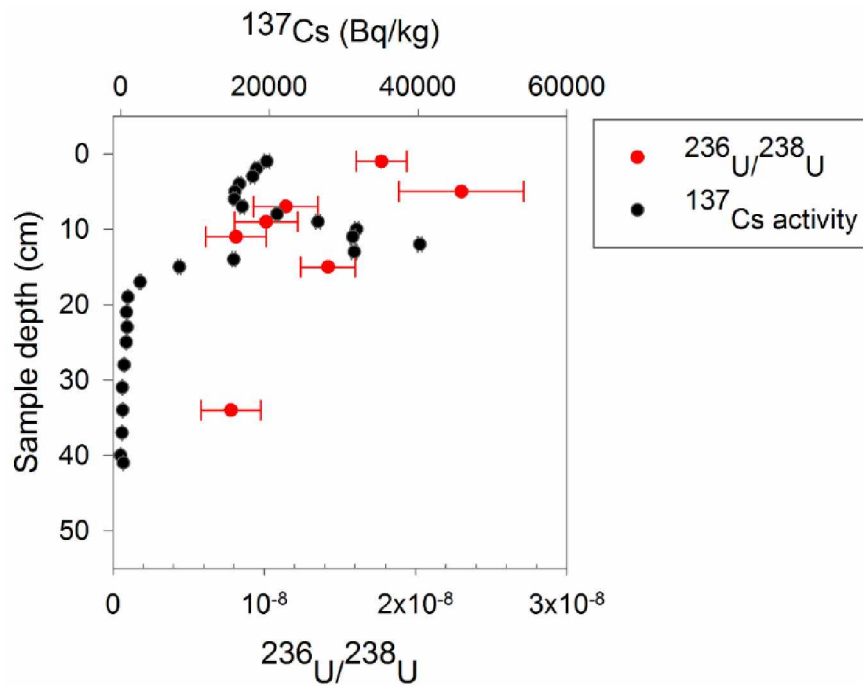
409

410 Data obtained with the two analytical methodologies were in very good agreement ( $R^2 = 0.99$ , slope of  
411 linear regression = 0.99) (Figure S2). The measured  $^{236}\text{U}/^{238}\text{U}$  isotope ratios ranged between  
412  $(7.33 \pm 2.20) \times 10^{-9}$  and  $(2.70 \pm 0.37) \times 10^{-8}$  (see Figure 3). These ratios were similar to the global fallout  
413 values ( $10^{-10} - 10^{-7}$ )(Sakaguchi et al., 2009; Schneider et al., 2017), relative to the FDNPP range  
414  $((3.42 \pm 0.52) \times 10^{-3})$ (Nishihara et al., 2012). The increase in  $^{236}\text{U}/^{238}\text{U}$  values observed in the upper  
415 section of the core is difficult to interpret because it may either reflect a slight impact of FDNPP derived  
416 U releases or a local heterogeneity of the U concentration in the environment. Nevertheless, it may be  
417 deduced from these measurements that the isotopic signature of U in these samples remained well  
418 within the range of global fallout so that the potential fallout from the FDNPP is not detectable in these  
419 samples. A part of U released from the FDNPP may also have been slowly incorporated into the bottom

420 sediment, which could explain the slight increase of the  $^{236}\text{U}/^{238}\text{U}$  isotope ratio observed in the upper  
421 part of the core and the absence of a peak similar to that recorded for radiocesium and Pu. Moreover,  
422 the geochemical behaviour of U may be different from that of radiocesium as it is likely contained in  $\text{UO}_2$   
423 microparticles from the nuclear fuel in association with Pu impurities. The absence of the detection of  
424 FDNPP –derived U suggested that the concentrations in actinide released from the power plant were  
425 lower than those already prevailing in the environment before the accident.

426

427



428

429 Figure 3: Evolution of the mean  $^{236}\text{U}/^{238}\text{U}$  atom ratios (red dots) and  $^{137}\text{Cs}$  activities (black dots) with depth in the  
430 Mano Dam sediment core. Uncertainties are extended with a coverage factor of 2. The uranium global fallout  
431 signature ( $10^{-10} - 10^{-7}$ ) falls beyond the range of the X-axis.

432

433



434 **Detectability of uranium releases from the FDNPP**

435

436 Although it was not possible to calculate the U source contributions as it was done for Pu, theoretical  
437 FDNPP-derived  $^{236}\text{U}$  concentrations ( $^{236}\text{U}_{\text{FDNPP}}$ ) in the samples analysed in the current study were  
438 estimated, based on the  $^{236}\text{U}/\text{Pu} = (0.46 \pm 0.12)$  ratio determined from the literature data (Nishihara et al.,  
439 2012). The maximum FDNPP-derived Pu concentration in soil samples analysed here reached  $30.7 \pm 9.4$   
440 fg/g (Table S5). Accordingly, the theoretical  $^{236}\text{U}$  concentration from the FDNPP was estimated to a  
441 maximum of  $14.1 \pm 5.6$  fg/g. Assuming a natural U concentration in Japanese soils of  $1.9 \pm 1.2$   
442  $\mu\text{g/g}$  (Yoshida et al., 1998; Yoshida et al., 2000), the estimation of the theoretical  $^{236}\text{U}_{\text{FDNPP}}/^{238}\text{U}$  (i.e. the  
443 potential impact of the FDNPP releases on the  $^{236}\text{U}/^{238}\text{U}$  measured in the samples) was  $(7.6 \pm 5.2) \times 10^{-9}$ .  
444 This theoretical calculation demonstrates that the occurrence of FDNPP-originating fallout is not  
445 detectable in the analysed samples, because there is no significant difference between the  $^{236}\text{U}_{\text{FDNPP}}/^{238}\text{U}$   
446 ratio in these sediment samples and the  $^{236}\text{U}/^{238}\text{U}$  isotope ratio associated with the very heterogeneous  
447 global fallout signal ( $10^{-10} - 10^{-7}$ ).

448 Similar calculations were performed to estimate the theoretical  $^{236}\text{U}$  concentrations in the sediment  
449 core, based on the FDNPP-derived Pu measurements in these samples. The resulting concentration  
450 amounts to 1.7 fg/g, which demonstrates that the FDNPP-originating U fallout did not reach the region  
451 of interest located at  $\sim 40$  km from the power plant. Nevertheless, the potential occurrence of U  
452 emissions by the FDNPP accident needs further investigations. In particular, similar analyses should be  
453 performed in more contaminated areas such as in sediment accumulated in lakes located closer to the  
454 FDNPP, where uranium may have been released in larger quantities.

455

456

457 **Acknowledgements:**

458

459 The collection and the analysis of the sediment samples were funded by the TOFU (ANR-11-JAPN-001)  
460 and the AMORAD (ANR-11-RSNR-0002) projects, funded by the French National Research Agency (ANR,  
461 *Agence Nationale de la Recherche*). Hugo Jaegler received a PhD fellowship from the French Atomic  
462 Energy Commission (CEA, Commissariat à l’Energie Atomique et aux Energies Alternatives). The authors  
463 are grateful to the Fukushima Agricultural Technology Centre for providing the soil samples collected  
464 before the FDNPP accident. The authors declare no competing financial interest

465

466

## 467 References

468

- 469 Bu, W., Zheng, J., Ketterer, M.E., Hu, S., Uchida, S., Wang, X. (2017) Development and application of mass  
470 spectrometric techniques for the ultra-trace determination of <sup>236</sup>U in environmental samples-A review.  
471 *Analytica Chimica Acta*.
- 472 Buesseler, K., Dai, M., Aoyama, M., Benitez-Nelson, C., Charmasson, S., Higley, K., Maderich, V., Masque,  
473 P., Oughton, D., Smith, J.N. (2016) Fukushima Daiichi-Derived Radionuclides in the Ocean: Transport,  
474 Fate, and Impacts. *Annual Review of Marine Science*.
- 475 Cao, L., Ishii, N., Zheng, J., Kagami, M., Pan, S., Tagami, K., Uchida, S. (2017) Vertical distributions of Pu  
476 and radiocesium isotopes in sediments from Lake Inba after the Fukushima Daiichi Nuclear Power Plant  
477 accident: Source identification and accumulation. *Applied Geochemistry* 78, 287-294.
- 478 Cao, L., Zheng, J., Tsukada, H., Pan, S., Wang, Z., Tagami, K., Uchida, S. (2016) Simultaneous  
479 determination of radiocesium ((135)Cs, (137)Cs) and plutonium ((239)Pu, (240)Pu) isotopes in river  
480 suspended particles by ICP-MS/MS and SF-ICP-MS. *Talanta* 159, 55-63.
- 481 Chartin, C., Evrard, O., Laceby, J.P., Onda, Y., Ottlé, C., Lefèvre, I., Cerdan, O. (2017) The impact of  
482 typhoons on sediment connectivity: lessons learnt from contaminated coastal catchments of the  
483 Fukushima Prefecture (Japan). *Earth Surface Processes and Landforms* 42, 306-317.
- 484 Chartin, C., Evrard, O., Onda, Y., Patin, J., Lefèvre, I., Ottlé, C., Ayrault, S., Lepage, H., Bonté, P. (2013)  
485 Tracking the early dispersion of contaminated sediment along rivers draining the Fukushima radioactive  
486 pollution plume. *Anthropocene* 1, 23-34.
- 487 Evrard, O., Laceby, J.P., Lepage, H., Onda, Y., Cerdan, O., Ayrault, S. (2015) Radiocesium transfer from  
488 hillslopes to the Pacific Ocean after the Fukushima Nuclear Power Plant accident: A review. *Journal of*  
489 *Environmental Radioactivity* 148, 92-110.
- 490 Evrard, O., Laceby, J.P., Onda, Y., Wakiyama, Y., Jaegler, H., Lefèvre, I. (2016) Quantifying the dilution of  
491 the radiocesium contamination in Fukushima coastal river sediment (2011–2015). *Scientific Reports* 6,  
492 34828.
- 493 Evrard, O., Pointurier, F., Onda, Y., Chartin, C., Hubert, A., Lepage, H., Pottin, A.C., Lefevre, I., Bonte, P.,  
494 Laceby, J.P., Ayrault, S. (2014) Novel insights into Fukushima nuclear accident from isotopic evidence of  
495 plutonium spread along coastal rivers. *Environmental Science & Technology* 48, 9334-9340.
- 496 Fukushima, T., Arai, H. (2014) Radiocesium contamination of lake sediments and fish following the  
497 Fukushima nuclear accident and their partition coefficient. *Inland Waters* 4, 2014 - 2214.
- 498 Hirose, K., Igarashi, Y., Aoyama, M., Miyao, T., (2001) Long-term trends of plutonium fallout observed in  
499 Japan, in: Kudo, A. (Ed.), *Radioactivity in the Environment*. Elsevier, pp. 251-266.
- 500 Huon, S., Hayashi, S., Laceby, J.P., Tsuji, H., Onda, Y., Evrard, O. (2018) Source dynamics of radiocesium-  
501 contaminated particulate matter deposited in an agricultural water reservoir after the Fukushima  
502 nuclear accident. *Science of The Total Environment* 612, 1079-1090.
- 503 Jaegler, H., Pointurier, F., Onda, Y., Hubert, A., Laceby, J.P., Cirella, M., Evrard, O. (2018) Plutonium  
504 isotopic signatures in soils and their variation (2011-2014) in sediment transiting a coastal river in the  
505 Fukushima Prefecture, Japan. *Environmental Pollution* 240, 167-176.
- 506 Kelley, J.M., Bond, L.A., Beasley, T.M. (1999) Global distribution of Pu isotopes and <sup>237</sup>Np. *Science of The*  
507 *Total Environment* 237–238, 483-500.
- 508 Kirchner, G., Bossew, P., De Cort, M. (2012) Radioactivity from Fukushima Dai-ichi in air over Europe;  
509 part 2: what can it tell us about the accident? *Journal of Environmental Radioactivity* 114, 35-40.
- 510 Kitamura, A., Kurikami, H., Sakuma, K., Malins, A., Okumura, M., Machida, M., Mori, K., Tada, K., Tawara,  
511 Y., Kobayashi, T., Yoshida, T., Tosaka, H. (2016) Redistribution and export of contaminated sediment

512 within eastern Fukushima Prefecture due to typhoon flooding. *Earth Surface Processes and Landforms*  
513 41, 1708-1726.

514 Kitamura, A., Yamaguchi, M., Kurikami, H., Yui, M., Onishi, Y. (2014) Predicting sediment and cesium-137  
515 discharge from catchments in eastern Fukushima. *Anthropocene* 5, 22-31.

516 Laceby, J.P., Evrard, O., Smith, H.G., Blake, W.H., Olley, J.M., Minella, J.P.G., Owens, P.N. (2017) The  
517 challenges and opportunities of addressing particle size effects in sediment source fingerprinting: A  
518 review. *Earth-Science Reviews* 169, 85-103.

519 Laceby, J.P., Huon, S., Onda, Y., Vaury, V., Evrard, O. (2016) Do forests represent a long-term source of  
520 contaminated particulate matter in the Fukushima Prefecture? *Journal of Environmental Management*  
521 183, 742-753.

522 Lee, S.H., La Rosa, J., Gastaud, J., Povinec, P.P. (2005) The development of sequential separation  
523 methods for the analysis of actinides in sediments and biological materials using anion-exchange resins  
524 and extraction chromatography. *Journal of Radioanalytical and Nuclear Chemistry* 263, 419-425.

525 Lepage, H., Laceby, J.P., Bonté, P., Joron, J.-L., Onda, Y., Lefèvre, I., Ayrault, S., Evrard, O. (2016)  
526 Investigating the source of radiocesium contaminated sediment in two Fukushima coastal catchments  
527 with sediment tracing techniques. *Anthropocene*.

528 Matsuda, K., Takagi, K., Tomiya, A., Enomoto, M., Tsuboi, J.-i., Kaeriyama, H., Ambe, D., Fujimoto, K.,  
529 Ono, T., Uchida, K., Morita, T., Yamamoto, S. (2015) Comparison of radioactive cesium contamination of  
530 lake water, bottom sediment, plankton, and freshwater fish among lakes of Fukushima Prefecture, Japan  
531 after the Fukushima fallout. *Fisheries Science* 81, 737-747.

532 Momoshima, N., Kakiuchi, H., Maeda, Y., Hirai, E., Ono, T. (1997) Identification of the contamination  
533 source of plutonium in environmental samples with isotopic ratios determined by inductively coupled  
534 plasma mass spectrometry and alpha-spectrometry. *Journal of Radioanalytical and Nuclear Chemistry*  
535 221, 213-217.

536 Muramatsu, Y., Yoshida, S., Tanaka, A. (2003) Determination of Pu concentration and its isotope ratio in  
537 Japanese soils by HR-ICP-MS. *Journal of Radioanalytical and Nuclear Chemistry* 255, 477-480.

538 Nishihara, K., Iwamoto, H., Suyama, K. (2012) Estimation of fuel compositions in Fukushima-Daiichi  
539 nuclear power plant. *JAEA-Data/Code 2012*, <http://jolissrch-inter.tokai-sc.jaea.go.jp/pdfdata/JAEA-Data-Code-2012-018.pdf> (2012)(Date of access: 29/02/2016).

540 Ohtsuka, Y., T., I., Kakiuchi, H., Y., T., Hisamatsu, S., J., I. (2004) Evaluation of  $^{239+240}\text{Pu}$ ,  $^{137}\text{Cs}$  and  
541 natural  $^{210}\text{Pb}$  fallout in agricultural upland fields in Rokkasho, Japan. *Journal of Radioanalytical and*  
542 *Nuclear Chemistry* 261, 625-630.

544 Sakaguchi, A., Kawai, H., Steier, P., Imanaka, T., Hoshi, M., Endo, I., Zhumadilov, K., M., Y. (2010)  
545 Feasibility of using  $^{236}\text{U}$  to reconstruct close-in fallout deposition from the Hiroshima atomic bomb.  
546 *Science of The Total Environment* 408, 5392 - 5398.

547 Sakaguchi, A., Kawai, K., Steier, P., Quinto, F., Mino, K., Tomita, J., Hoshi, M., Whitehead, N., Yamamoto,  
548 M. (2009) First results on  $^{236}\text{U}$  levels in global fallout. *Science of The Total Environment* 407, 4238-4242.

549 Sakaguchi, A., Steier, P., Takahashi, Y., Yamamoto, M. (2014) Isotopic Compositions of  $^{236}\text{U}$  and Pu  
550 Isotopes in "Black Substances" Collected from Roadsides in Fukushima Prefecture: Fallout from the  
551 Fukushima Dai-ichi Nuclear Power Plant Accident. *Environmental Science & Technology* 48, 3691-3697.

552 Salbu, B. (2011) Radionuclides released to the environment following nuclear events. *Integrated*  
553 *Environmental Assessment and Management* 7, 362-364.

554 Schneider, S., Bister, S., Christl, M., Hori, M., Shozugawa, K., Synal, H.-A., Steinhauser, G., Walther, C.  
555 (2017) Radionuclide pollution inside the Fukushima Daiichi exclusion zone, part 2: Forensic search for the  
556 "Forgotten" contaminants Uranium-236 and plutonium. *Applied Geochemistry*.

557 Schneider, S., Walther, C., Bister, S., Schauer, V., Christl, M., Synal, H.-A., Shozugawa, K., Steinhauser, G.  
558 (2013) Plutonium release from Fukushima Daiichi fosters the need for more detailed investigations.  
559 *Scientific Reports* 3.

560 Schwantes, J.M., Orton, C.R., Clark, R.A. (2012) Analysis of a Nuclear Accident: Fission and Activation  
561 Product Releases from the Fukushima Daiichi Nuclear Facility as Remote Indicators of Source  
562 Identification, Extent of Release, and State of Damaged Spent Nuclear Fuel. *Environmental Science &*  
563 *Technology* 46, 8621-8627.

564 Shinonaga, T., Steier, P., Lajos, M., Ohkura, T. (2014) Airborne Plutonium and Non-Natural Uranium from  
565 the Fukushima DNPP Found at 120 km Distance a Few Days after Reactor Hydrogen Explosions.  
566 *Environmental Science & Technology* 48, 3808-3814.

567 Tanaka, K., Iwatani, H., Sakaguchi, A., Fan, Q., Takahashi, Y. (2015) Size-dependent distribution of  
568 radiocesium in riverbed sediments and its relevance to the migration of radiocesium in river systems  
569 after the Fukushima Daiichi Nuclear Power Plant accident. *Journal of Environmental Radioactivity* 139,  
570 390-397.

571 Tanimizu, M., Sugiyama, N., Ponzevera, E., Bayon, G. (2013) Determination of ultra low  $^{236}\text{U}/^{238}\text{U}$  isotope  
572 ratios by tandem quadrupole ICP-MS. *Journal of Analytical Atomic Spectrometry* 28, 1372-1376.

573 Trémillon, B. (1965) *Les séparations par les résines échangeuses d'ions*. Gauthier-Villars.

574 Xu, C., Zhang, S., Sugiyama, Y., Ohte, N., Ho, Y.F., Fujitake, N., Kaplan, D.I., Yeager, C.M., Schwehr, K.,  
575 Santschi, P.H. (2016) Role of natural organic matter on iodine and Pu distribution and mobility in  
576 environmental samples from the northwestern Fukushima Prefecture, Japan. *Journal of Environmental*  
577 *Radioactivity* 153, 156-166.

578 Yamada, S., Kitamura, A., Kurikami, H., Yamaguchi, M., Malins, A., Machida, M. (2015) Sediment and  $^{137}\text{Cs}$   
579 transport and accumulation in the Ogaki Dam of eastern Fukushima. *Environmental Research Letters* 10,  
580 014013.

581 Yamamoto, M., Sakaguchi, A., Ochiai, S., Takada, T., Hamataka, K., Murakami, T., Nagao, S. (2014)  
582 Isotopic Pu, Am and Cm signatures in environmental samples contaminated by the Fukushima Dai-ichi  
583 Nuclear Power Plant accident. *Journal of Environmental Radioactivity* 132, 31-46.

584 Yamamoto, M., Takada, T., Nagao, S., Koike, T., Shimada, K., Hoshi, M., Zhumadilov, K., Shima, T.,  
585 Fukuoka, M., Imanaka, T., Endo, S., Sakaguchi, A., Kimura, S. (2012) An early survey of the radioactive  
586 contamination of soil due to the Fukushima Dai-ichi Nuclear Power Plant accident, with emphasis on  
587 plutonium analysis. *Geochemical Journal* 46, 341-353.

588 Yamashiki, Y., Onda, Y., Smith, H.G., Blake, W.H., Wakahara, T., Igarashi, Y., Matsuura, Y., Yoshimura, K.  
589 (2014) Initial flux of sediment-associated radiocesium to the ocean from the largest river impacted by  
590 Fukushima Daiichi Nuclear Power Plant. *Scientific Reports* 4, 3714.

591 Yang, G., Tazoe, H., Yamada, M. (2016) Determination of  $^{236}\text{U}$  in environmental samples by single  
592 extraction chromatography coupled to triple-quadrupole inductively coupled plasma-mass spectrometry.  
593 *Analytica Chimica Acta*.

594 Yoshida, S., Muramatsu, Y., Tagami, K., Uchida, S. (1998) Concentrations of lanthanide elements, Th, and  
595 U in 77 Japanese surface soils. *Environment International* 24, 275-286.

596 Yoshida, S., Muramatsu, Y., Tagami, K., Uchida, S., Ban-nai, T., Yonehara, H., Sahoo, S. (2000)  
597 Concentrations of uranium and  $^{235}\text{U}/^{238}\text{U}$  ratios in soil and plant samples collected around the uranium  
598 conversion building in the JCO campus. *Journal of Environmental Radioactivity* 50, 121 - 172.

599 Zhang, Y., Zheng, J., Yamada, M., Wu, F., Igarashi, Y., Hirose, K. (2010) Characterization of Pu  
600 concentration and its isotopic composition in a reference fallout material. *Science of The Total*  
601 *Environment* 408, 1139-1144.

602 Zheng, J., Tagami, K., Bu, W., Uchida, S., Watanabe, Y., Kubota, Y., Fuma, S., Ihara, S. (2014)  $^{135}\text{Cs}/^{137}\text{Cs}$   
603 isotopic ratio as a new tracer of radiocesium released from the Fukushima nuclear accident.  
604 *Environmental Science & Technology* 48, 5433-5438.

605 Zheng, J., Tagami, K., Watanabe, Y., Uchida, S., Aono, T., Ishii, N., Yoshida, S., Kubota, Y., Fuma, S., Ihara,  
606 S. (2012b) Isotopic evidence of plutonium release into the environment from the Fukushima DNPP  
607 accident. *Scientific Reports* 2, 304.

